

## The Mount Edgecumbe Tephra Deposits, a Marker Horizon in Southeastern Alaska near the Pleistocene–Holocene Boundary

JAMES R. RIEHLE,\* DANIEL H. MANN,† DOROTHY M. PETEET,‡  
DANIEL R. ENGSTROM,§ DAVID A. BREW,|| AND CHARLES E. MEYER¶

\*U.S. Geological Survey, 4200 University Drive, Anchorage, Alaska 99508; †Quaternary Research Center, University of Washington, Seattle, Washington 98195; ‡Goddard Institute for Space Studies, 2880 Broadway, New York, New York, 10025; §Limnological Research Center, University of Minnesota, Minneapolis, Minnesota 55455; and ||U.S. Geological Survey MS 904 and, ¶U.S. Geological Survey MS 975, 345 Middlefield Road, Menlo Park, California 94025

Received August 29, 1990

Late Pleistocene tephra deposits found from Sitka to Juneau and Lituya Bay are assigned to a source at the Mount Edgecumbe volcanic field, based on similarity of glass compositions to near-vent deposits and on thinning away from Kruzof Island. The sequence of near-vent layers is basaltic andesite and andesite at the base, rhyolite, and mixed dacite and rhyolite on top. The only breaks in the tephra sequence are two 1-mm-thick silt partings in a lake-sediment core, indicating a depositional interval from basaltic andesite to dacite of no more than about a millennium. Tephra deposits at sites >30 km from the vent are solely dacite and rhyolite and are 10,600 to 11,400 <sup>14</sup>C yr old based on interpretation of 18 radiocarbon ages, including 5 by accelerator mass spectrometry (AMS). Basaltic andesite and andesite deposits nearer the vent are as much as 12,000 yr old.

Discrepancy among radiocarbon ages of upland tephra deposits provisionally correlated as the same grainfall is resolvable within  $\pm 2\sigma$  of analytical uncertainty. Comparison of bulk and AMS ages in one sediment core indicates a systematic bias of +600 to +1100 yr for the bulk ages; correlation of tephra deposits among upland and lacustrine sites implies an additional discrepancy of 200–400 yr between upland (relatively too young) and lacustrine ages. In any case, the Mount Edgecumbe tephra deposits are a widespread, latest Pleistocene stratigraphic marker that serves to emphasize the uncertainty in dating biogenic material from southeastern Alaska. © 1992 University of Washington.

### INTRODUCTION

Late Quaternary tephra (fallout ash) deposits at Lituya Bay, Juneau, and Sitka in southeastern Alaska were described by Heusser (1960), McKenzie (1970), Yehle (1974), Mann (1983), and Mann and Ugolini (1985), all of whom suggested that the deposits had a source at the Mount Edgecumbe volcanic field (MEF) on Kruzof Island (Fig. 1). Seamounts in the Gulf of Alaska and Quaternary volcanoes elsewhere in southeastern Alaska are more distant than the MEF (Brew *et al.*, 1984; Rossman, 1959), which was thus a more reasonable candidate for the source area. Yehle (1974) described beds of different colors in a sequence of tephra layers at Sitka, indicating a range of compositions. Four radiocarbon ages relating to the tephra deposits

have been published:  $8570 \pm 300$  yr B.P. for a tree rooted atop tephra deposits at Sitka (W-1739; Yehle, 1974);  $9150 \pm 150$  and  $9180 \pm 150$  yr B.P. for a tree on the west coast of Kruzof Island buried by one of the youngest deposits (I-12,218 and I-12,219; Riehle and Brew, 1984);  $10,300 \pm 400$  yr B.P. for peat beneath a tephra bed near Juneau (L-297D; Heusser, 1960); and a composite age of 11,000 yr B.P. (see below) based on correlation of a tephra layer among several sites near Glacier Bay (McKenzie, 1970) (Fig. 1).

As the five of us independently pursued studies of surficial deposits in southeastern Alaska and volcanic deposits on Kruzof Island, we found that the age of the latest Pleistocene tephra layers appeared to differ among localities. In this paper we pool our recently acquired data, correlate tephra

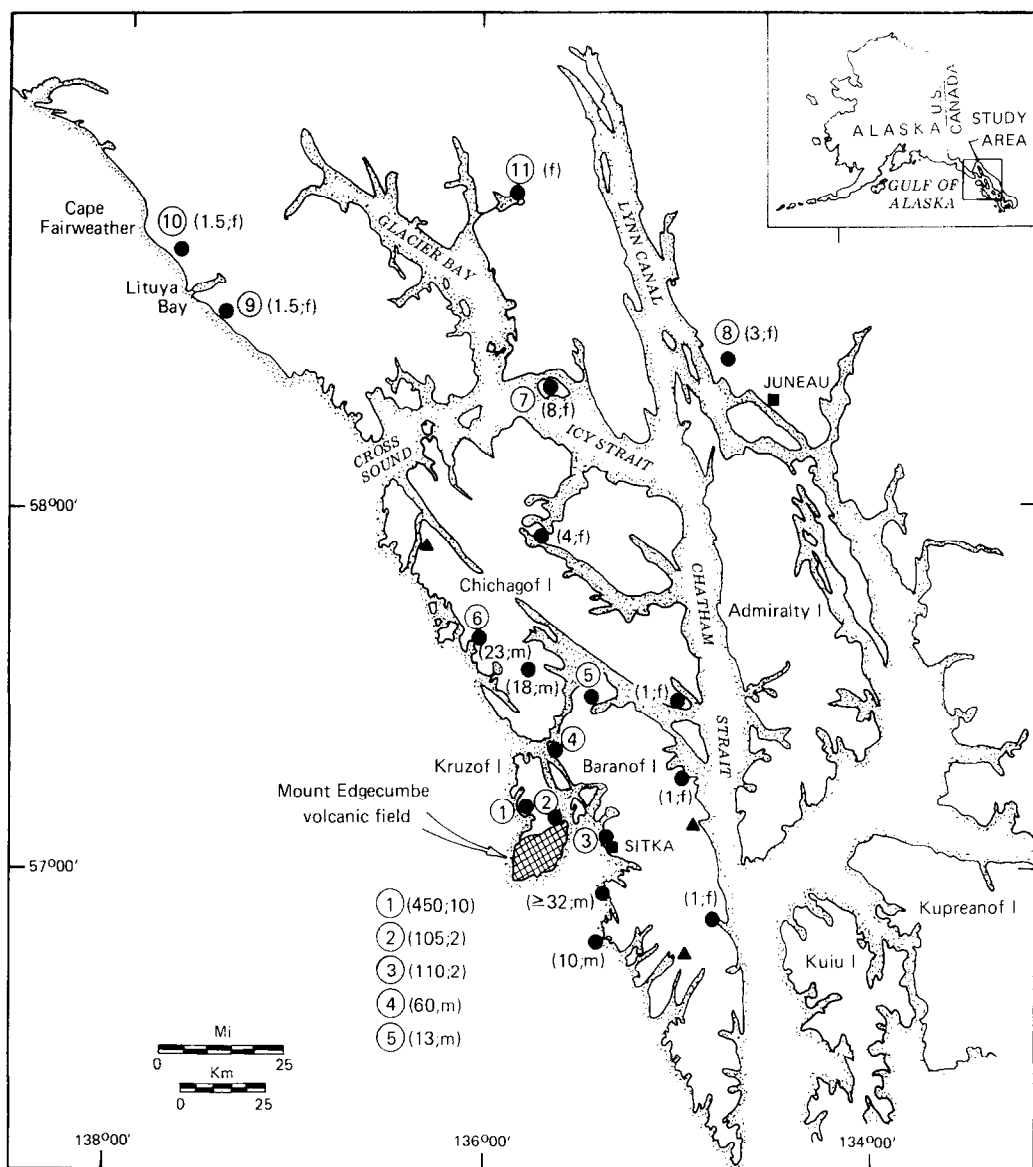


FIG. 1. Location of the Mount Edgecumbe volcanic field on southern Kruzof Island in southeastern Alaska. The localities of regional tephra deposits described in this report are shown as numbered dots. Deposit thickness (cm) is given in parentheses, followed by median grain size (mm) based on sieving or by "m" or "f" (for medium- or fine-grained ash) by visual estimation. Dots having only numbers in parentheses are sites where a tephra deposit occurs but is not described in detail; triangles are sites where tephra was sought but not found.

samples from several sites, and interpret the radiocarbon data to propose an age range for the sequence of tephra layers.

#### STRATIGRAPHY OF THE MOUNT EDGECUMBE VOLCANIC FIELD

The Mount Edgecumbe volcanic field is

30 km west of Sitka (Fig. 1). The field has two main volcanic landforms—the composite cone of Mount Edgecumbe and the crater and domes of Crater Ridge—and several smaller scoria cones (Fig. 2). The geologic section on southern Kruzof Island consists of Pleistocene lava flows (Riehle *et al.*, 1989) overlain by pyroclastic-flow and fall-

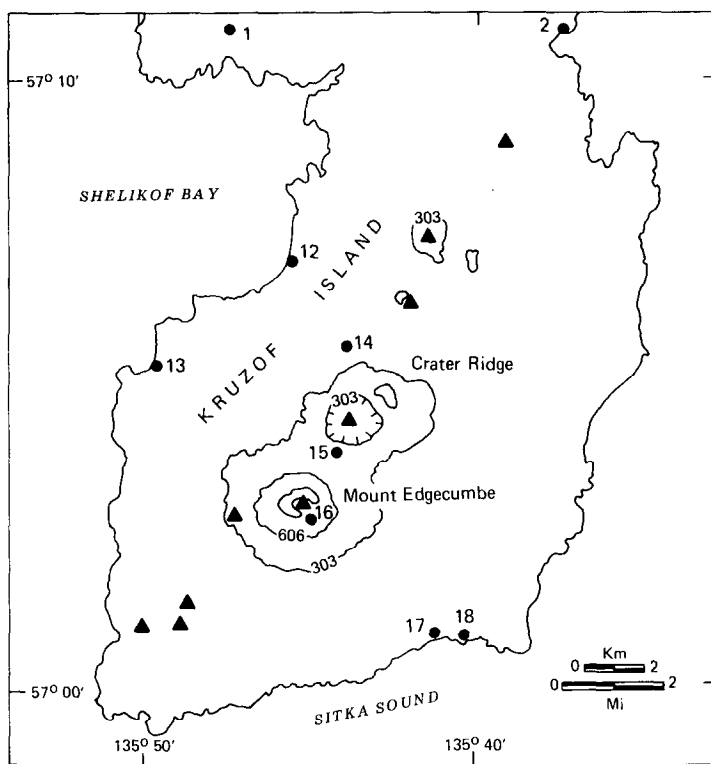


FIG. 2. Map of southern Kruzof Island showing the composite cone of Mount Edgecumbe, the domes and crater of Crater Ridge, and smaller scoria cones. Triangles are volcanic vents active following deglaciation; numbered dots are sites of near-vent fallout or pyroclastic-flow samples described in the text or tables. Contour interval 303 m (1000 ft). Base from U.S.G.S. quadrangles Sitka A-5 and A-6 (1951; scale 1:63, 360).

out deposits (J. Riehle, unpublished data). Till occurs locally between the lava flows and the pyroclastic deposits, indicating that most of the cones and craters are postglacial in age. The exact age of deglaciation of Kruzof Island is unknown; deglaciation of the region had begun no later than 12,500 yr ago (Mann, 1986).

The oldest postglacial pyroclastic deposits are beds of red and dark-gray basaltic andesite scoria (51–57%  $\text{SiO}_2$ , bulk) that are overlain by beds of grayish-brown andesitic scoria (57–63%  $\text{SiO}_2$ ). Such mafic fallout deposits occur only as far as 30 km to the north of the MEF (site 6, Fig. 1). The most widespread MEF pyroclasts are fallout deposits of dacitic (66–70%  $\text{SiO}_2$ , bulk) and rhyolitic (>70%  $\text{SiO}_2$ ) composition. Rhyolitic fallout and pyroclastic flows were erupted from Crater Ridge repeatedly over a period of at least a few hundred years, as

implied by different directions of the natural remanent magnetization of the deposits (D. Champion, written communication, 1990). Andesitic eruptions of Mount Edgecumbe began before and continued after the onset of rhyolitic eruptions, and a major dacitic eruption of Mount Edgecumbe occurred after the last andesitic eruption but before the last rhyolitic eruption of Crater Ridge. Dacitic tephra deposits are 10 m thick 20 km northwest of Mount Edgecumbe (sites 12 and 13, Fig. 2) and none have been found to the south or east.

Two small-volume pyroclastic eruptions between about 6000 and 4000 yr ago (Riehle and Brew, 1984) resulted in one, or uncommonly two, closely adjacent beds of fine-grained rhyolitic tephra on Kruzof Island and nearby sites. Away from Kruzof Island the beds are typically a pale-gray parting only a few millimeters thick in the soil over-

lying the main sequence of tephra deposits. There is little chance of mistaking such middle Holocene deposits, known only within 75 km of Kruzof Island, for the widespread latest Pleistocene tephra deposits which are the focus of this paper.

#### SAMPLE LOCALITIES AND ANALYTICAL METHODS

Tephra samples obtained at 11 sites in southeastern Alaska (Figs. 1 and 3) are the basis for this paper. Two sites on Kruzof Island and a site 20 km to the east at Sitka are near-vent sites where bedding is well preserved and there is little contamination of the thick, coarse tephra deposits by loess or organic matter. The middle Holocene tephra deposits are found at these sites. Sites 4–7 are lakes or ponds and sites 8–11 are upland peat deposits. Tephra was recovered from lakes and bogs using a modified Livingston corer.

Tephra samples (letter labels, Fig. 3) were cleaned by boiling and (or) ultrasonic agitation for 10 min, wet-sieved, and oven-dried before weighing and examination by binocular microscope. Juvenile pumiceous clasts were selected by sieving or picking and were repetitively and gently crushed and sieved to 0.05–0.10 mm. The sieved fraction was then washed to get rid of adhering fines. The dried sample was subjected to one or more cycles of separation in heavy liquids (methylene iodide) and in a magnetic separator. Examination by polarizing microscope indicated that separates are typically >99% glass.

Glass separates were analyzed for 9 major elements by electron microprobe. Each analysis (Table 1) is an average of 6 to 12 analyses of individual shards. Some shard analyses were discarded for inclusion of mineral microlites, which are readily recognized by a concurrent increase in some elements (Na, Ca, and Al in the case of plagioclase) and a proportional decrease of other elements. Uncommonly, other shard analyses were discarded for having the extreme value for each of 3 or more elements

in the range of values for the sample. The dense fraction ( $>2.60 \text{ g/cm}^3$ ) of each sample was microscopically examined to determine its phenocryst content (Table 2).

#### CORRELATIONS AMONG NEAR-VENT AND DISTAL SAMPLES

##### *Glass Composition as a Basis for Correlation*

We use the similarity of glass compositions as a basis for correlating the tephra deposits. Minerals can fractionate by grain size and density during transport in the airborne plume. Moreover, silicic tephra deposits of MEF have only a small percentage of plagioclase and trace amounts of pyroxene and amphibole (Table 2) and so their mineral content is inadequate to distinguish among numerous deposits. Bulk composition is not used for correlation because the separation of mineral grains from glass during transport leads to a change of bulk composition (Sarna-Wojcicki *et al.*, 1981). Glass is likely to have the same composition (or compositional range) throughout a deposit. Minor elements in glass can be used for correlation (e.g., Sarna-Wojcicki *et al.*, 1980) but they are typically used to distinguish among evolved rhyolites that, unlike MEF magmas, have highly similar major-element contents. Major elements are readily determined by microprobe and serve as a threshold test for similarity.

We compare glass compositions by means of a similarity coefficient ( $sc$ ) (Borchardt *et al.*, 1972), calculated as the average ratio of the normalized oxides of two samples where the lesser oxide is the numerator. Because analytical uncertainty is inversely proportional to abundance (Table 1), we exclude from the calculation any oxide having an abundance less than an arbitrary 0.40%. Our analytical uncertainty is calculated for the spread of background-corrected peak counts and includes the effects of variable hydration as well as low total counts caused by inadvertent analysis of occult microvesicles. The total effect of

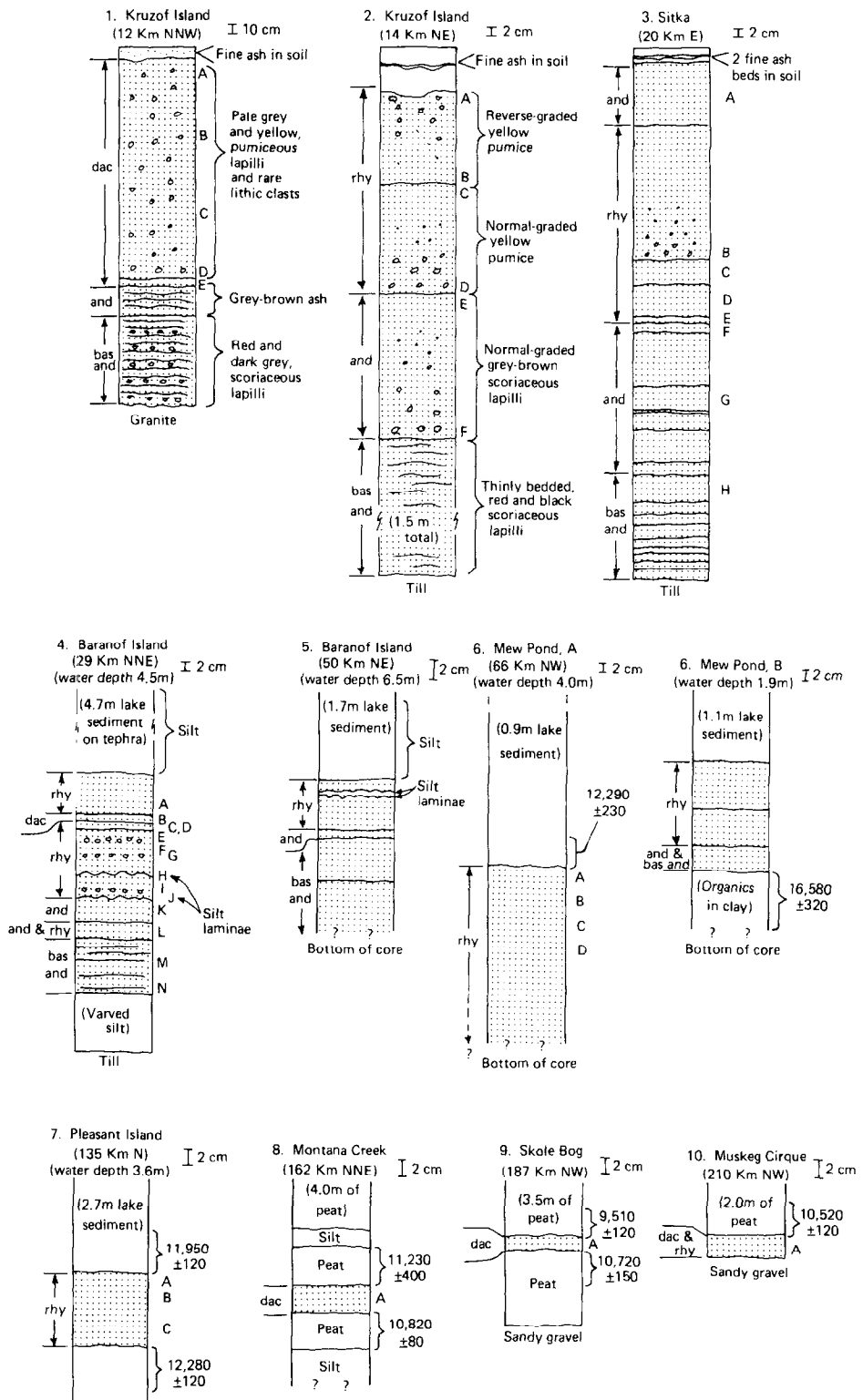


FIG. 3. Measured sections at sites of tephra deposits shown on Figure 1; distance of each site from vents on southern Kruzof Island is given in parentheses. Horizontal lines indicate bedding breaks in tephra deposits (light shading). Lapilli-size clasts are indicated by small circles. Sites 4 through 7 are lake-sediment cores. Tephra samples are indicated by letter labels; radiocarbon ages in yr B.P. are selected from Table 5. Note the different scales for each section. Abbreviations: and, andesitic; bas and, basaltic andesite; dac, dacitic; rhy, rhyolitic.

TABLE 1. COMPOSITIONS OF GLASS SEPARATES FROM REPRESENTATIVE NEAR-VENT DACITIC AND RHYOLITIC PYROCLASTS OF THE MOUNT EDGE-CUMBE VOLCANIC FIELD, ALASKA. ONE STANDARD DEVIATION AS A PERCENTAGE OF THE REPORTED VALUE IS IN PARENTHESES AFTER EACH ANALYSIS; NO VALUES ARE GIVEN FOR MNO WHICH OCCURS IN ABUNDANCES NEAR THE LIMIT OF DETECTABILITY. SITE LOCALITIES ARE SHOWN ON FIGURES 1 AND 2

[Analyst: J. Riehle. ARL SEM9 9-channel microprobe or, where "No. shards" is in parentheses, 3-channel ARL EMX-3M. Analyses done at U.S.G.S., Menlo Park. Operating conditions: 15 kv, .01 microamp sample current on brass, defocused beam and 20-second count times to minimize loss of alkalis. Each analysis is an average of multiple analyses of individual shards, the number of shards given after the total for each sample. Standards: synthetic andesite glass ("GSC") for Na, Mg, Ca, K, and Fe; natural rhyolitic glass ("ST2") for Si and Al; synthetic TiO<sub>2</sub> and synthetic Mn<sub>2</sub>O<sub>3</sub> (9-channel instrument) for Ti and Mn, or natural hornblende and rhodonite (3-channel instrument) for Ti and Mn. Use of trade names is for descriptive purposes only and does not constitute a product endorsement by the U.S. Geological Survey]

Site	rhyolitic		pyroclastic flow		rhyolitic		dacitic fallout deposits					
	2R112b	2R136y	2-C	1R46d	5R3a1	5R3a2	5R3c	1R75a	1R75a'	1R75a	1R75a	1R75a'
SiO <sub>2</sub>	69.6(2.1)	69.3(1.7)	70.6(2.9)	69.6(1.3)	68.3(1.5)	68.5(1.9)	64.5(1.6)	63.7(3.3)	69.1(3.9)	70.7(2.1)		
Al <sub>2</sub> O <sub>3</sub>	15.2(2.5)	13.3(2.9)	13.3(2.6)	14.9(4.0)	15.6(3.6)	14.2(3.3)	15.1(2.1)	15.6(3.1)	14.6(3.9)	14.6(3.3)		
FerOs	3.73(13)	2.75(6.7)	2.65(5.4)	4.05(12)	5.04(5.8)	2.89(4.1)	4.29(4.6)	4.65(6.0)	3.93(13)	3.57(11)		
MgO	0.59(4.0)	0.21(21)	0.26(8.9)	0.33(29)	0.82(8.6)	0.32(12)	0.93(9.7)	1.11(7.0)	0.75(7.2)	0.32(5.0)		
CaO	2.53(5.4)	1.48(11)	1.69(9.1)	2.08(8.1)	3.21(14)	2.01(14)	3.44(6.0)	3.68(7.4)	2.98(8.3)	1.98(7.0)		
Na <sub>2</sub> O	4.25(6.5)	4.80(5.3)	3.87(7.4)	4.94(4.2)	5.44(4.7)	3.72(10)	4.15(11)	4.21(8.9)	4.67(5.8)	4.67(3.4)		
K <sub>2</sub> O	2.25(9.8)	2.41(5.6)	2.35(4.6)	2.29(17)	1.14(24)	2.24(5.5)	1.74(9.1)	1.63(6.0)	1.95(9.2)	2.04(9.5)		
TiO <sub>2</sub>	0.41(33)	0.32(14)	0.22(10)	0.54(19)	0.70(17)	0.25(35)	0.57(11)	0.64(7.5)	0.53(30)	0.43(25)		
MnO	0.06	0.05	0.04	0.06	0.07	0.05	0.07	0.07	0.07	0.05		
Total	98.6	94.6	95.0	98.8	100.3	94.2	94.8	94.8	99.0	98.4		
No. shards	(24)	(30)	8	(26)	(23)	10	4	12	(24)	(23)		
SiO <sub>2</sub> normalized to 100 percent	70.6	73.3	71.6	70.4	68.1	72.7	68.0	67.2	69.8	71.8		

2R112b: pale yellow, highly vesicular subround lapilli handpicked from nonsorted ash-flow tuff

2R136y: pale gray or yellow, highly vesicular angular lapilli handpicked from well sorted fallout deposits of mixed pumice, dense dark gray lithics, and ash

2-C: pale gray, highly vesicular angular pumice handpicked from well sorted pumice and ash

1R46d, 1R46d: light gray and dark gray bands, respectively, from block of moderately vesicular, banded vitrophyre

5R3a1, 5R3a2: major and minor components of a single pale yellow-brown, moderately vesicular, pumiceous lapillus picked from

a well sorted fallout deposit at least 5 m thick

5R3c: a single pumice lapillus picked 4 m below 5R3a

TABLE 2. GLASS COMPOSITIONS AND PETROGRAPHIC DESCRIPTIONS OF REPRESENTATIVE DISTAL TEPHRA DEPOSITS, UNMELTED LUMINA, AND CHANNEL MICROPROBE; OPERATIONAL DETAILS SAME AS IN HEADING FOR TABLE 1. THE PETROGRAPHIC DESCRIPTIONS SHOULD BE USEFUL FOR PRELIMINARY CLASSIFICATION OF TEPHRA SAMPLES COLLECTED IN THE FUTURE

Site	dacitic fallout		rhyolitic fallout		4-D	Description
	1-C	10-AZ	10	4		
SiO <sub>2</sub>	69.7(1.9)	69.2(0.6)	70.7(0.8)	71.0(1.6)	4-A: anhedral plagioclase>>euhedral orthopyroxene>clinopyroxene; rare apatite (?); about 40% opaque clots and pale brown glass	
Al <sub>2</sub> O <sub>3</sub>	14.7(2.9)	15.4(2.2)	14.2(3.0)	14.0(3.1)	4-B: plagioclase>euhedral orthopyroxene>clinopyroxene; about 40% opaque minerals, opaque clots, and pale brown glass	
FerO <sub>3</sub>	3.42(13)	3.61(3.2)	2.79(3.8)	2.73(8.9)	4-C: angular plagioclase>clinopyroxene>orthopyroxene, some glass-coated; 50% opaque clots and pale brown glass	
MgO	0.52(33)	0.61(4.3)	0.30(9.8)	0.28(35)	4-D: subhedral plagioclase>>pyroxene; about 60% vitrophyre fragments, opaque clots, and pale brown glass	
CaO	2.34(20)	2.50(1.4)	1.89(3.0)	1.70(5.7)	4-E: anhedral plagioclase>>orthopyroxene=clinopyroxene; rare apatite and hornblende; about 40% opaque clots and pale brown glass	
Na <sub>2</sub> O	4.64(2.0)	3.78(2.9)	4.60(3.1)	4.63(2.1)	4-F: plagioclase chips>euhedral orthopyroxene>clinopyroxene; about 40% vitrophyre clasts, opaque clots, and pale brown glass	
K <sub>2</sub> O	2.08(10)	1.97(1.9)	2.25(1.6)	2.38(3.1)	4-G: anhedral plagioclase>>orthopyroxene=clinopyroxene; rare zircon(?); about 50% opaque clots and pale brown glass	
TiO <sub>2</sub>	0.39(25)	0.41(11)	0.25(20)	0.26(21)	4-H: anhedral plagioclase>>orthopyroxene>clinopyroxene; rare hornblende and apatite; 50% opaque clots and pale brown glass	
MnO	0.06	0.06	0.07	0.07	4-I: anhedral plagioclase>euhedral orthopyroxene>clinopyroxene; rare apatite; 50% opaque clots and pale brown glass	
Total	97.9	97.5	97.1	97.1	4-J: anhedral plagioclase>>orthopyroxene=clinopyroxene; rare hornblende and apatite; 50% vitrophyre fragments and pale brown glass	
No. shards	7	10	13	9	4-K: plagioclase>euhedral orthopyroxene>clinopyroxene; rare apatite; 50% vitrophyre clasts and pale brown glass	
SiO <sub>2</sub> normalized to 100 percent	71.2	71.0	72.8	73.1	8-A: plagioclase>>euhedral orthopyroxene>clinopyroxene; rare hornblende and apatite; 50% vitrophyre clasts and pale brown glass [glass is megascopically pale brown, but in transmitted light is essentially colorless; clast shapes range from blocky plates having discrete microvesicles, to those having slightly drawn out bubbles, to fibrous but not highly vesicular pumice]	
					9-A: plagioclase fragments>>euhedral orthopyroxene; rare anhedral hornblende; about 50% devitrified vitrophyre clasts and pale brown glass [glass is megascopically pale yellow-brown, in transmitted light clear to faintly yellow-brown; shapes range from curvilinear plates, some having a single rib of a relict bubble wall, to murky and massive microvesicular blocks, to highly foliated but not highly vesicular pumice]	
					10-A: angular or euhedral plagioclase>>euhedral orthopyroxene=subhedral hornblende; rare clinopyroxene, apatite; 50% murky brown vitrophyre or pale brown glass [glass is megascopically very pale brown, in transmitted light is clear to faintly tinted brown; shapes range from single-rib curvilinear plates, to massive microvesicular, to strongly foliated, moderately vesicular pumice]	

hydration, other elements not included in the analysis, and microvesicles is removed by calculating the *sc* using major-element contents normalized to 100%.

The minimum value of *sc* necessary to support correlation depends on the compositional variability that remains after normalization. Such remaining variability includes both actual compositional variability and instrumental variability. We have periodically analyzed splits of glass separates (Table 3); the *sc*'s of the high-silica glass splits are 0.97–0.99, which we treat as a practical approximation of the instrumental variability. Thus, *sc*'s of high-silica glasses that are less than about 0.98 indicate real differences. Splits of low-silica glasses have lower *sc*'s (0.97–0.94; Table 3) which probably indicate a higher degree of compositional heterogeneity; the low-silica glasses typically have some microlites even after multiple cycles of separation. Even in the low-silica glass splits, however, average oxide values are well within the calculated analytical uncertainty of one another.

Clearly the degree of compositional heterogeneity can vary with sample size: individual lapilli (and derived shards) can be finely banded, can vary throughout an eruption, or, like the (informal) Mazama ash (Smith and Westgate, 1969), can be homogeneous and constant in composition throughout an eruption. In contrast, Downes (1985) found that glass in each lapillus in a dacitic tephra deposit in the Yukon Territory has a composition that varies within analytical uncertainty. Variations between lapilli or between individual shards of a bulk sample, however, exceed analytical uncertainty and thus indicate heterogeneous magma.

To identify two samples as the same grainfall, cutoff values of *sc* can be empirically derived for each source area by analysis of multiple samples. As shown below, 0.95 seems to be a suitable cutoff for the *rhyolitic* MEF pyroclasts; an *sc* <0.95 means that correlation is unlikely and a value of 0.95 is ambiguous. Not all of the

numerous rhyolitic tephra layers, however, are uniquely distinguishable by major-element contents. Thus, a value of *sc* >0.95 does not ensure correlation as the same grainfall. In contrast, *dacitic* MEF pyroclasts are more heterogeneous than the rhyolitic pyroclasts and many samples of a single dacitic grainfall have *sc* values with one another of only 0.90–0.95.

Our main objective is to identify samples that are highly similar to one another. For brevity, we show only a few glass analyses selected to be representative (Table 1) but we include *sc* values for all pairs among our sample set (Table 4).

#### *Compositions and Heterogeneity of Near-Vent Fallout Deposits*

The dacitic fallout deposit is a single bed that is 10 m thick on the west shore of Kruf Island (sites 12 and 13, Fig. 2). Analyses of multiple glass separates from within banded lapilli or between adjacent lapilli indicate that the dacitic glass is heterogeneous, ranging from 68% SiO<sub>2</sub> (normalized) to 73% SiO<sub>2</sub>. Samples 1R46l and 1R46d (Table 1; SiO<sub>2</sub> 70.4 and 68.1%), for example, are light and dark bands from a single lapillus. Similarly, 5R3a1 and 5R3a2 are two glass components in a single lapillus. Sample 5R3a2 is a more similar to 5R3c, a single lapillus from lower in the same fallout deposit, than to 5R3a1. These dacitic glasses are only marginally similar to one another, most having *sc*'s <0.95 (Table 4A). Correlation of these samples as the same grainfall based on glass composition alone is uncertain owing to such heterogeneity.

The rhyolitic tephra deposits comprise several compositional groups, samples of each group having *sc*'s ≥0.95 with one another (clusters of high *sc* in Table 4B). At some sites, succeeding layers are highly similar to one another (e.g., 3-B, C, D, and E; Table 4B). Some compositions occur only in certain azimuths: for example, deposits to the north of the vent (1-E and 2-A-B-C) are dissimilar to those to the east (3-B-C-D; Table 4B). The rhyolitic pyro-

TABLE 3. REPLICATE MICROPROBE ANALYSES OF SPLITS OF GLASS SEPARATES TO ILLUSTRATE REPRODUCIBILITY  
 [Conditions as reported in Table 1. Analysts: G.E. Meyer and J.R. Fiehle. Samples 2K168b and 1R070e by 3-channel EMX-SM.  
 all others by 9-channel SEMq. Use of trade names is for descriptive purposes only and does not constitute a product  
 endorsement by the U.S. Geological Survey.]

	Standard RUS132, rhyolitic glass												
	2K168b	1R070e	3R185c	2R112e	Ave. of 3 analyses		Ave. of 18 analyses		Norm.	wet			
					through 1/86 to 100% through 4/87 to 100% chemistry		through 4/87 to 100% chemistry						
SiO <sub>2</sub>	62.1	61.8	61.7	61.8	69.3	69.1	70.3	71.1	75.3(0.2%)	76.4	75.4(0.8%)	76.3	75.7
Al <sub>2</sub> O <sub>3</sub>	16.6	16.6	16.9	17.3	14.9	14.7	13.7	14.0	11.3(1.2%)	11.5	11.3(1.4%)	11.4	11.4
FerO <sub>s</sub>	7.12	7.06	7.40	7.40	2.61	2.59	2.66	2.77	2.34(0.2%)	2.37	2.33(1.9%)	2.36	2.33
MgO	2.14	1.99	1.64	1.55	0.48	0.48	0.28	0.28	0.04(12%)	0.04	0.06(18%)	0.06	0.05
CaO	4.60	4.75	5.15	4.32	1.65	1.64	1.63	1.72	0.11(2.3%)	0.11	0.11(9.1%)	0.11	0.12
Na <sub>2</sub> O	4.78	4.65	5.09	5.40	5.12	5.09	4.30	4.40	4.74(1.3%)	4.81	4.88(2.7%)	4.94	5.25
K <sub>2</sub> O	1.25	1.14	1.15	1.40	3.00	3.00	2.39	2.34	4.45(0.3%)	4.49	4.42(1.4%)	4.47	4.53
TiO <sub>2</sub>	1.31	1.29	1.52	1.56	0.46	0.49	0.24	0.25	0.19(5.4%)	0.19	0.19(5.3%)	0.19	0.21
MnO	0.12	0.11	0.09	0.10	0.15	0.15	0.05	0.06	0.13(3.1%)	0.13	0.16(6.2%)	0.16	0.15
total	100.0	99.4	100.6	100.8	97.7	97.2	95.6	96.9	98.6	98.8	98.8	98.8	99.8
No. shards	(27)	(30)	(25)	(27)	8	10	9	12					
s.c.	0.97	0.94			0.99		0.98						





clasts are less heterogeneous than the dacitic pyroclasts, and on a larger scale than single lapilli.

To illustrate better the nature of the compositional heterogeneity of these glasses, compositions of individual glass shards are shown (Fig. 4). Two components are clearly identifiable in dacitic sample 5R3a based on bimodal MgO and  $\text{Fe}_7\text{O}_3$  contents. The analytical uncertainties of oxides in the major component (5R3a1) are not improved by normalization, indicating that most of its variability is actual. Indeed, 5R3a1 has no sc in excess of 0.92 with any other sample (and so is not in Table 4A). Conversely, dacitic sample 1-A is unimodal (Fig. 4B) and its analytical uncertainties, especially that of  $\text{SiO}_2$ , are improved by normalization (Table 4A).

### Compositions of the Distal Fallout Samples

Dacitic tephra has been identified (Table 4A) at distal sites 4, 6, 7, 8, 9, 10, and 11 (Fig. 1). Despite the close proximity of their sites northwest of the vent, samples 9-A and 10-A1 are only marginally similar to one another ( $sc = 0.93$ ) and to the other dacitic samples (Table 4A). Dacitic samples from sites 4, 6, 7, 8, and 11 north-northeast of the vent are similar to one another: most sc's are 0.95 to 0.98. All distal dacitic samples are approximately similar to at least one near-vent sample, but only three distal samples have an  $sc > 0.95$  with any proximal sample (samples 9-A, 2-D, and 6-D2). Perhaps the distal deposits formed of limited parts of a broadly heterogeneous

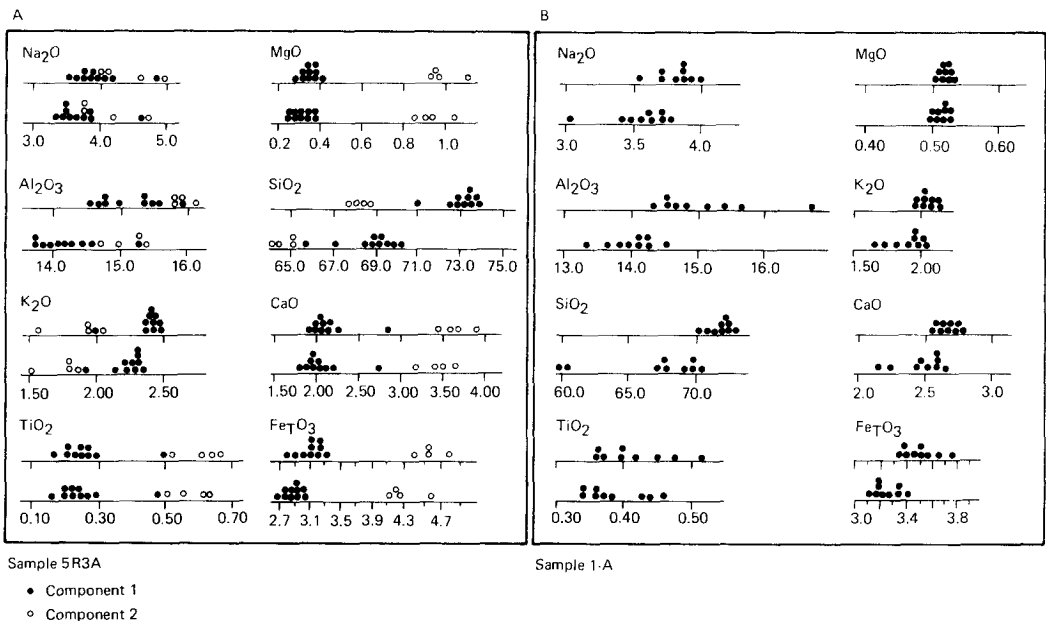


FIG. 4. Histograms showing the distribution of major oxide abundances (in wt%) in individual glass shards of Mount Edgecumbe fallout deposits. In each plot, the lower line shows raw abundances and the upper line shows abundances after normalization to 100 percent. (A) Two glass components can be identified in dacitic lapillus 5R3a based on normalized MgO, SiO<sub>2</sub>, CaO, and Fe<sub>7</sub>O<sub>3</sub>. Normalization does not improve variability, indicating that much of the analytical uncertainty represents actual chemical heterogeneity (1  $\sigma$  relative before/after normalization of component 1 is: Na<sub>2</sub>O, 10/9.3%; MgO, 12/12%; Al<sub>2</sub>O<sub>3</sub>, 3.3/3.0%; SiO<sub>2</sub>, 1.9/1.1%; K<sub>2</sub>O, 5.7/5.8%; CaO, 15/12%; TiO<sub>2</sub>, 35/34%; Fe<sub>7</sub>O<sub>3</sub>, 4.3/4.7%). (B) The composition of dacitic ash 1-A is unimodal and the analytical uncertainty, especially of SiO<sub>2</sub>, is improved by normalization (1 $\sigma$  before/after normalization is: Na<sub>2</sub>O, 6.6/3.6%; MgO, 10/6.7%; Al<sub>2</sub>O<sub>3</sub>, 2.7/5.1%; SiO<sub>2</sub>, 6.0/0.3%; K<sub>2</sub>O, 6.6/2.8%; CaO, 7.3/3.3%; TiO<sub>2</sub>, 12/13%; Fe<sub>7</sub>O<sub>3</sub>, 3.1/3.9%). Thus, much of the analytical uncertainty is the effect of hydration and (or) microvesicles and is removed by normalization.

eruption column during brief energetic pulses.

Except at site 8, dacitic ash at all other distal localities is mixed with rhyolitic ash. At site 4, layer 4-B is pure dacitic ash but dacitic ash is mixed with rhyolitic ash in the over- and underlying layers (4-A and 4-C). Such mixing may occur secondarily by freeze-thaw, or may indicate overlapping falls of dacitic and rhyolitic ash. At no site, however, is there more than one dacitic grain-fall deposit (i.e., two layers of dacitic ash separated by a layer of rhyolitic ash).

Most rhyolitic samples at sites to the northwest, northeast, and east of the MEF (Sites 1-3, Fig. 1) have sc's with one another that are  $\leq 0.95$  and so represent different eruptions of distinguishable magmas. In contrast, some different eruptions produced similar deposits: 4-A1 and 4-L1, the youngest and oldest rhyolitic deposits at site 4, have an sc of 0.96 with one another yet are clearly not the same grainfall deposit.

Based on occurrence of bedding breaks and differences in glass composition, six groups of rhyolitic layers can be distinguished in a lake basin northeast of the vent (site 4, Fig. 3). These are, from oldest: 4-L1 (rhyolitic ash mixed with andesitic ash), G-H-I-J (includes a silt parting), F, C2-D-E (also includes a parting), and A1. Layers 4-G-H-I-J and C2-D-E each comprise two grainfalls but because of their high degree of chemical similarity, we treat G-H-I-J together as a group and C2-D-E as another group. Layers 4-A2, 4-B, and 4-C1 are dacitic ash.

Four layers of rhyolitic ash occur east of the vent (site 3, Fig. 3). The layers are chemically similar to one another (sc  $\geq 0.96$ ; 3-B, C, D, and E, Table 4B) and constitute a group that is similar to rhyolitic deposits C2-D-E and G-H-I-J at site 4 and to parts of chemically heterogeneous deposits at distal sites 6 and 7 north of the vent (Table 4B). Proximal rhyolitic deposits north of the vent are one thick, chemically homogeneous bed (2-A-B-C, Fig. 3) that overlies a thin bed (2-D) of dacitic ash, and

a thin rhyolitic bed (1-E, Fig. 3) that underlies a thick deposit of dacitic ash (1-A-B-C-D).

Despite the lack of bedding within the deposit at site 7, glass in subsample 7-A is chemically distinguishable from that in 7-B and 7-C (Table 4B). Thus, the deposit is a composite of multiple grainfalls; bedding is not discernible probably due to fine grain size and bioturbation.

#### *Proposed Correlations*

We propose correlation of the samples from different sites as the same grainfall based on their compositional similarity and stratigraphic position. Sites 4, 6, 7, and 11 are nearly colinear with the source, thus each deposit at the more distant sites 7 and 11 should have a correlative at site 6 and (or) at site 4. Indeed, except for sample 7-A, all rhyolitic samples at sites 4, 6, and 7 are nearly indistinguishable (Table 4B). The proposed correlatives of the rhyolitic samples are outlined in Table 4. Because of the large number of measured sections and deposits, we have not outlined the proposed correlatives on Figure 3 as well; colored pencils might aid in doing so.

We propose the following correlatives: (1) 3-B-C-D and 4-G-H-I-J; (2) 2-A-B-C, 4-F(?), and 11-1; (3) 1-A-B-C, 2-D(?), and 11-2; (4) 6-A-C1-D1, 7-B-C2, and 4-C2-D-E. Rhyolitic deposits 2-A, 2-B, and 2-C overlie dacitic deposit 2-D, and deposit 4-F underlies all dacitic ash at site 4. If there was but a single dacitic grainfall, then one of 4-F and 2-D cannot correlate as proposed above. Our data cannot resolve this dilemma. The lowest dacitic ash at site 4 is mixed in layer C and we correlate this ash (C1) with the lowest dacitic ash at the other distal sites: (5) 4-C1, 6-C2, 7-C1, and probably 8-A. Rhyolitic ash 10-A2 matches all rhyolitic deposits at site 4 equally well but due to its occurrence mixed with dacitic ash (10-A1) we favor correlation of 10-A2 with upper layers 4-A1 or 4-C2-D-E.

#### *Discussion of Correlations*

Despite ambiguity in correlations of

some samples, all distal samples are broadly similar in glass composition to one or more near-vent samples. Thickness and grain-size data are also consistent with an origin at MEF for all samples (Fig. 1).

To summarize, the oldest rhyolitic tephra (4-L1) was deposited north of the vent and mixed with andesitic tephra (Fig. 5A). Two to four rhyolitic grainfalls occurred after a brief hiatus and include a brief hiatus (silt partings at site 4; Fig. 3). Ash from these eruptions was distributed east and north-

east of the vent (3-B-C-D-E, 4-G-H-I-J, 6-D1, and 7-C2; Fig. 5B). Rhyolitic and dacitic eruptions then produced tephra deposits that extend northwest (sites 11 and 12), north and north-northeast (sites 1, 2, and 4; correlatives at sites 6, 7, 8, 9, 10, and 11) of Mount Edgecumbe. For two reasons we infer that these eruptions were simultaneous. First, dacitic ash and rhyolitic ash are mixed within individual layers at sites 4, 6, 7, 10, and 11. Second, simple correlations having consistent stratigraphic rela-

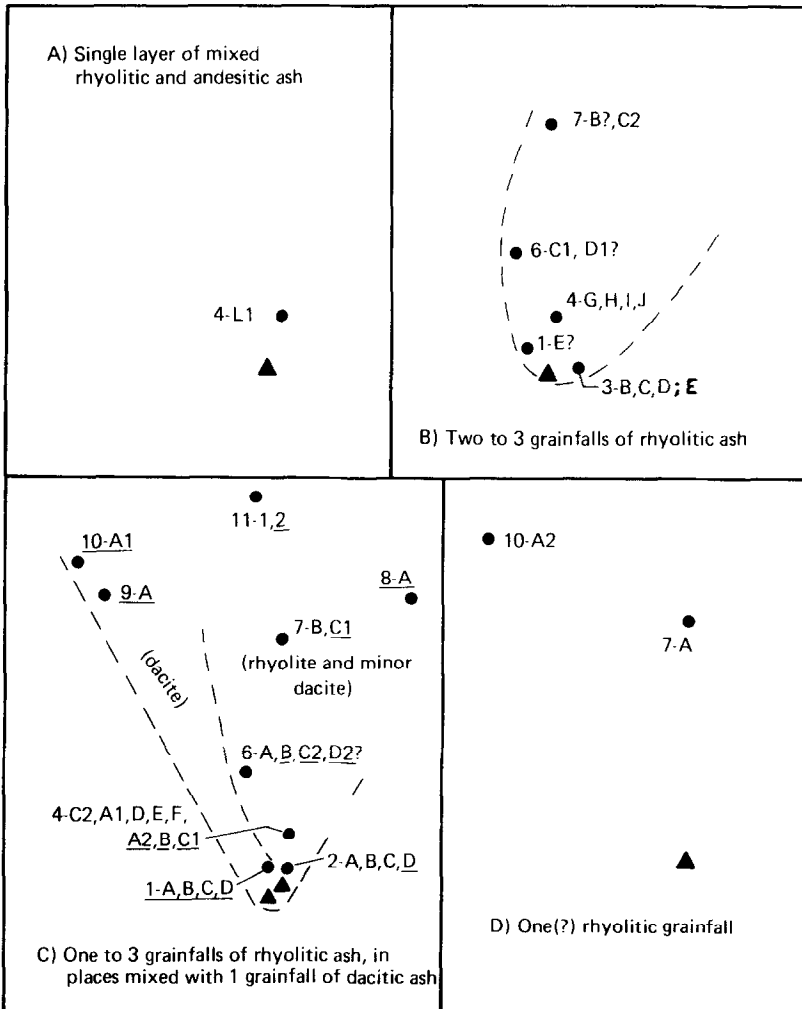


FIG. 5. Schematic summary of correlations among silicic tephra deposits of the Mount Edgecumbe volcanic field, from oldest (A) to youngest (D). The source (triangles) of the dacitic fallout is Mount Edgecumbe and the source of the rhyolitic fallout is Crater Ridge. Our data are inadequate to define precisely the edge of each plume, thus dashed lines are only a conceptual approximation.

tions cannot be deduced among the dacitic and uppermost rhyolitic ash deposits at sites 1, 2, and 4. The total of the evidence is that there was but a single dacitic eruption. Thus, we hypothesize that dacitic ash fell initially at site 2 (2-D) but near the vent was subsequently confined to the southwest of an interface between plumes of rhyolitic ash (2-A-B-C and 4-F) and dacitic ash (1-A-B-C-D; Fig. 5C). Late in the concurrent eruptions, high-flung rhyolitic ash (4-C2-D-E) and dacitic ash (4-C1-B) each eventually fell at site 4 in a succession reflecting earlier pulsing of each eruption column.

Rhyolitic ash occurs mixed with dacitic ash in the topmost deposit at sites 4 (4-A1) and 7 (7-A), and 7-A is possibly correlative with rhyolitic ash 10-A2. This youngest deposit of rhyolitic ash may have formed either by the last fall of fine ash erupted concurrently with the dacitic ash or by a separate rhyolitic eruption after the dacitic eruption. There are no topmost rhyolitic layers at sites 1 and 2 that correlate with 4-A1 or 7-A (Fig. 5D), thus we prefer the former alternative.

#### AGE OF THE TEPHRA DEPOSITS

Radiocarbon ages that bound the MEF tephra deposits range from 16,500 to 9200 yr B.P. (Table 5). Although the large number of deposits may support a protracted eruptive period, we doubt that the age range is as large as 7300 yr. Lake sediments at site 4 (Fig. 3) include a compositionally complete tephra sequence from basaltic andesite at the base to rhyolite at the top. Only two laminae of silt, each about 1 mm thick, occur within the entire tephra sequence. We do not know how long after each eruption sedimentation was dominated by eroded tephra; assuming reworking for 100 yr, the 6 rhyolitic deposits could represent as many as 600 yr. This is a *maximum* estimate because we have seen no evidence in the deposits for reworking (color changes or clast rounding that grade upward within an ash bed). The 4.8 m of

lake sediment deposited over about 10,000 yr represent an average rate of 0.5 mm/yr, so the 2 silt partings probably represent only a few decades. We believe the entire tephra sequence at site 4, including the basaltic andesite layers, was deposited in less than a millennium. We do have an accelerator-mass-spectrometry (AMS) age beneath the tephra deposits, but the analytical uncertainty at  $2\sigma$  ( $16,500 \pm 6400$  yr B.P.; Table 5) is too large to aid in confirming the hypothesis.

Both bulk-sediment and AMS ages were obtained for lake sediments including the MEF tephra deposits on Pleasant Island (site 7) (Table 5). Bulk ages indicate that sedimentation rates varied in different parts of the core (Fig. 6). More important, three AMS ages of conifer needles indicate a discrepancy with bulk ages of 600 to 1000 yr in one part of the core and 700 to 1100 yr in another part of the core. Such an older shift of bulk sediment ages has been reported elsewhere (Lowe *et al.*, 1988) and here is probably due mainly to input of ancient carbon (as bicarbonate ion) from tills in the catchment basin and potentially to sedimentary contamination by older biogenic carbon. A fourth AMS age of an unidentified woody fragment falls on the depth-age curve established by adjacent ages of bulk organic sediments. It is 400–500 yr older than the two AMS ages of conifer needles from deeper in the core. We have no certain explanation for this discrepancy but speculate that the woody material may have been contaminated by aquatic carbon or may be reworked from older material in the drainage basin.

The tephra deposit on Pleasant Island (site 7) is closely bounded by bulk sample ages of  $11,950 \pm 120$  yr B.P. above and  $12,280 \pm 120$  yr B.P. below (Table 5). We correlate the tephra deposit at site 7 with the uppermost rhyolitic deposits at site 4 (4-E through 4-A) but the glass analyses do not preclude the possibility that older rhyolitic ash (4-F or G-H-I-J) occurs at site 7 as well. In any case, the maximum difference

TABLE 5. RECENTLY ACQUIRED RADIOCARBON AGES LIMITING THE MOUNT EDGECUMBI TEPHRA DEPOSITS; ACCELERATOR-MASS-SPECTROMETRY AGES INDICATED BY ASTERISK. AGES FOR LOCALITY 7, PLEASANT ISLAND, ARE PLOTTED ON FIGURE 6; ALL OTHERS ARE PLOTTED ON FIGURE 3.

Locality (Fig. 1)	Laboratory	Age (yr)	Stratum (Sample Material)	Sample Locality
7	WIS-1958	8330±80	6-cm interval of organic muck (gyttja), 144-148 cm	pond 500 ft elev. on Pleasant Is.; 58°01'20" 135°37'10" (Bureau B quadrangle)
7	WIS-1947	10,110±100	8-cm interval of organic muck (gyttja), 182-190 cm	as above
7	WIS-2100	10,530±110	8-cm interval of organic muck (gyttja), 210-218 cm	as above
7	WIS-1948	11,620±120	8-cm interval of organic muck (gyttja), 244-252 cm	as above
7	WIS-1949	11,950±120	6-cm interval of organic muck (gyttja), 262-268 cm, immediately above tephra	as above
7	WIS-1950	12,280±120	8-cm interval of organic muck (gyttja), 176-280 cm, immediately below tephra	as above
7	WIS-1951	13,760±120	8-cm interval of organic muck (gyttja), 296-304 cm	as above
7	ETH-4734*	9080±105	spruce needles sieved from 1-cm interval, 181-183 cm	as above
7	ETH-8076*	11,430±120	unidentified woody fragment, 14-cm	as above
7	ETH-8694*	11,640±100	pine needles, 118 cm	as above
7	ETH-8895*	10,480±90	pine needles, 154 cm	as above
6	Beta 4673B	12,130±130	3-cm interval of organic muck (gyttja) immediately above tephra	Mew Pond; 57°39'49" 138°00'48" 2 km E of Chicagof, Sitka 17 quadrangle; 100 ft as.
6	AA 4141*	16,580±2000	Cyperus seed picked from 6-cm organic rich clay interval	as above
8	U.S.G.S-2961	11,230±400	1-cm peat horizon	upper Montana Creek, 810 ft elev.; 58°28'04" 134°41'35" (Bureau B quadrangle)
8	U.S.G.S-2968	10,820±80	1-cm peat horizon	as above
8	Beta 4988	8510±110	3-cm peat horizon, immediately above tephra, some root contamination	600 ft. km SE of Lituya Bay at 580 ft elev.; 58°34'18" 138°17'37" (Mount Fairweather 9 quadrangle)
8	Beta 4987	10,720±130	3-cm peat horizon, immediately below tephra, some root contamination	as above
10	Beta 4518	13,520±120	3-cm peat horizon, immediately above tephra, some root contamination	600 ft. km NW of Lituya Bay at 1680 ft elev.; 58°44'54" 137°44'38" (Mount Fairweather 9 quadrangle)

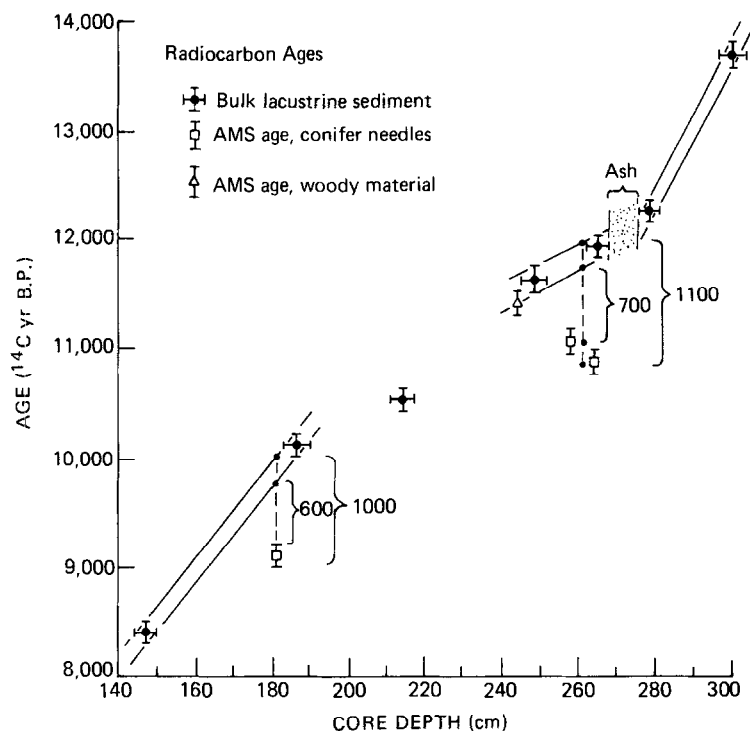


FIG. 6. Bulk and accelerator-mass-spectrometry (AMS) radiocarbon ages in yr B.P. of lake sediments from Pleasant Island near Glacier Bay (site 7, Figs. 1 and 3) plotted against core depth. Bulk ages are older than true ages because of sedimentologic and geochemical processes; an estimate of the amount of bias (600–1100 yr) is provided by three AMS-age determinations on conifer needles.

in the bulk ages at site 7 ( $330 \pm 240$  yr) is consistent with our previous estimate of 600 yr maximum for the entire rhyolitic sequence at site 4.

The AMS-adjusted age ranges from site 7 are plotted on Figure 7 together with the radiocarbon data from other sites. The interpreted probable age range of the deposits at site 7 is between about 11,000 and 11,400 yr B.P. (double-ruled area), but owing to propagation of analytical uncertainty, it could be as large as 10,600 to 11,800 yr B.P. The three Montana Creek age determinations are consistent with one another within  $\pm 2\sigma$  if the actual age is between 10,400 and 11,000 yr B.P.; the same composite age results, even excluding Heusser's (1960) early age. Rhyolitic ash at site 6 is limited by a bulk age of lacustrine gyttja to  $>12,290 \pm 230$  yr B.P. (Table 5) but given the demonstrated error in the Pleasant Island bulk ages, this age is uncertain for being potentially too old as well.

A sample of the tephra layer at Glacier Bay was provided by G. D. McKenzie (sample 11, Table 4). The layer occurs near the top of emergent marine deposits which are limited by two bulk ages from sites adjacent to that where the tephra layer occurs (McKenzie, 1970):  $10,940 \pm 155$  yr B.P. (I-2395) for overlying basal peat and  $10,400 \pm 260$  yr B.P. (I-1616) for rooted wood. McKenzie also reports the age of a conifer cone in the marine deposits, but its stratigraphic position is not precisely given and the cone could be as much as a century older than the sediments. The minimum limiting peat age is the same as that from Pleasant Island, about 10,600 yr (Fig. 7).

The dacitic tephra deposit at site 10 has an upper limiting age of  $10,520 \pm 120$  yr B.P. and at site 9 is limited by  $9510 \pm 105$  yr B.P. above and  $10,720 \pm 150$  yr B.P. below (Table 5). These composite limits (10,200 to 11,000 yr B.P.) are slightly younger than those from Montana Creek. The deposit at

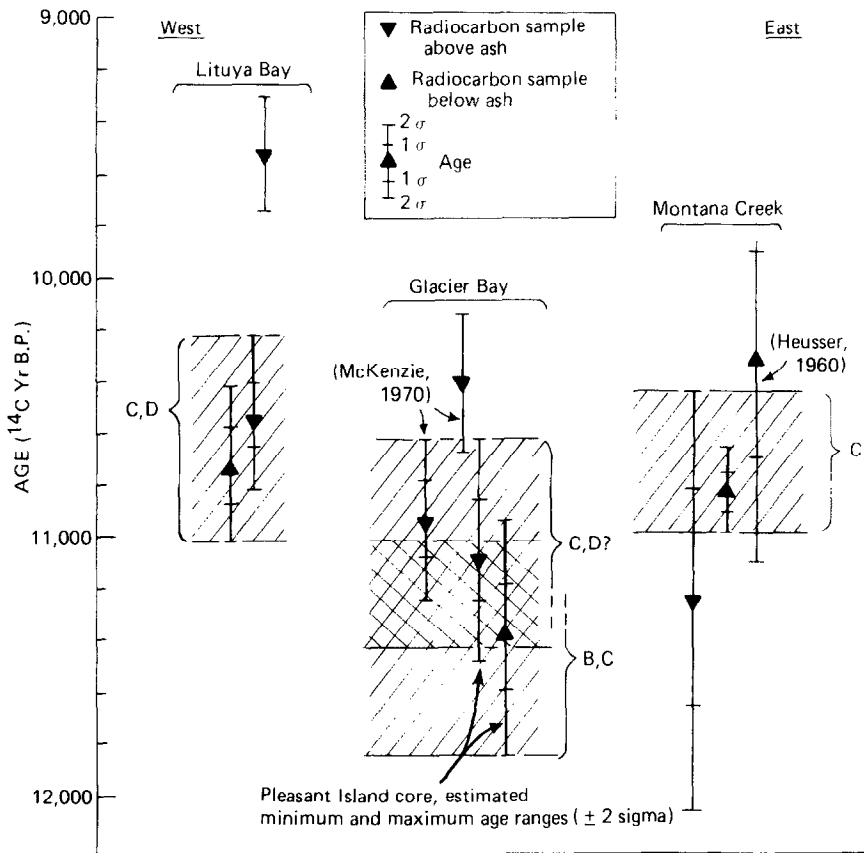


FIG. 7. Schematic summary of radiocarbon ages that limit the age range of the latest Pleistocene silicic fallout deposits of the Mount Edgecumbe volcanic field. Samples are arranged in order of locality from west to east: Lituya Bay (sites 9 and 10, Fig. 1); Glacier Bay (sites 7 and 11); and Montana Creek (site 8). Diagonals are the permissible age range of deposits based on the combined  $2\sigma$  analytical uncertainty of all plotted ages at each locality. Propagation of error in AMS-based corrections to bulk ages in the Pleasant Island core results in unusually large uncertainty. The double diagonals are the likely age range of the tephra deposits in the Pleasant Island core and the single diagonals are the extreme possible range. Capital letters refer to the groupings of tephra deposits based on correlations shown in Figure 5 from oldest (B) to youngest (D).

site 7, however, is estimated to be not younger than 10,600 yr B.P. (Fig. 7) and it includes dacitic ash. Thus, the estimated composite age of the dacitic tephra deposit based on all available data from sites 7, 9, 10, and 11 is 10,600–11,000 yr B.P.

Data from site 7 alone imply that the dacitic ash is probably between 11,000 and 11,400 yr old (Fig. 7). Although the bulk age samples closely bound the tephra layer at site 7, they are subject to a large degree of uncertainty due to propagation of errors introduced in their correction by use of the more accurate AMS ages. Either (1) the

composite range of 10,600–11,000 yr for the dacitic ash is correct and is simply at the upper limit of the range of site-7 age data, (2) there remains a systematic bias of 200 to 400 yr between the ages of terrestrial and lacustrine samples (the terrestrial ages being too young), or (3) the tephra deposit at site 7 includes dacitic ash as young as 10,600–11,000 yr B.P. as well as rhyolitic ash as old as 11,000–11,400 yr old (correlative with 4-G-H-I-J). Future work may resolve this uncertainty.

The last of these latest Pleistocene–early Holocene eruptions occurred about 9160 yr

ago based on the age of a stump (Riehle and Brew, 1984) buried by the uppermost of the pyroclastic deposits on the west shore of Kruzof Island (site 12, Fig. 2). The top of the stump was frayed and the tree had probably been killed by the deposit. The only fallout samples that might correlate with such a young eruption are 4-A and 10-A2. We have previously argued, however, that 10-A2 is >10,600 yr old (Fig. 7). Most probably, if the eruption 9200 yr ago produced an ash plume, it extended west to the sea.

### SUMMARY AND CONCLUSIONS

The latest Pleistocene deposits of dacitic and rhyolitic tephra occur widely in the northern part of southeastern Alaska. Chemically heterogeneous dacitic pyroclasts comprise the deposit of a single grainfall. Rhyolitic pyroclasts comprise multiple layers, each of which is more homogeneous than the dacitic deposit. The variability of the major elements in glass as determined by microprobe is insufficient to permit unambiguous correlation of some rhyolitic layers. General similarity to glass in near-vent samples, however, together with trends of grain size and deposit thickness, support correlation of all dacitic and rhyolitic samples with the Mount Edgecumbe volcanic field on Kruzof Island.

The range of radiocarbon ages associated with these silicic tephra deposits is 9200 to 16,500 yr B.P. but the nearly total absence of internal unconformities implies an age range of no more than a millennium and perhaps only decades. Comparison of bulk ages with AMS ages shows that bulk lake-sediment ages from Pleasant Island are too old by 600–1100 yr. Moreover, replicate ages of terrestrial deposits at Montana Creek serve to emphasize that the true age may differ from the reported age by two or even three times the analytical uncertainty of one  $\sigma$  (more if the sample is contaminated). Eighteen radiocarbon ages can be interpreted to limit the age of the silicic tephra deposits to between 10,600 and 11,400 yr B.P. Part of this range of 600 yr

may be due to a potential discrepancy of 200–400 yr that remains between ages of terrestrial samples (relatively too young) and AMS-corrected ages of lacustrine samples.

Within 30 km to the north of Kruzof Island, the silicic tephra deposits immediately overlie tephra deposits of andesitic and basaltic andesite composition. The lack of unconformities within these mafic fallout deposits implies that the oldest mafic deposit is no more than about 12,000 yr old.

Despite ambiguities in correlations of some silicic samples, the sequence of MEF tephra deposits should be useful as a latest Pleistocene stratigraphic marker in the region from Kruzof Island to the northeast as far as Juneau and northwest as far as Lituya Bay. In particular, there are no other tephra deposits in the region with which they can be confused. Our attempts to date the deposits precisely serve to emphasize the uncertainties inherent in the radiocarbon method. We suggest that future work in southeastern Alaska include additional radiocarbon dating to confirm or refine the age range of the tephra deposits. It is also important to continue evaluating the suitability of sample material from the region for dating by systematically comparing bulk ages with those acquired by AMS techniques.

### ACKNOWLEDGMENTS

Careful reviews by Thomas Hamilton, David Hopkins, Andrei Sarna-Wojcicki, and William Scott resulted in significant improvements to the manuscript. One of us (Engstrom) was supported in this work by NSF Grant BSR-8705371.

### REFERENCES CITED

- Borchardt, G. A., Aruscavage, P. J., and Millard, H. T., Jr. (1972). Correlation of the Bishop ash, a Pleistocene marker bed, using instrumental neutron activation and analysis. *Journal of Sedimentary Petrology* 42, 301–306.
- Brew, D. A., Ovenshine, A. T., Karl, S. M., and Hunt, S. J. (1984). "Preliminary reconnaissance geologic map of the Petersburg and parts of the Port Alexander and Sumdum 1:250,000 quadrangles,

- southeastern Alaska." Geological Survey Open-File Report 84-405.
- Downes, Hilary (1985). Evidence for magma heterogeneity in the White River ash (Yukon Territory). *Canadian Journal of Earth Sciences* 22, 929-934.
- Engstrom, D. R., Hansen, B. C. S., and Wright H. E., Jr. (1990). A possible Younger Dryas record in southeastern Alaska. *Science* 250, 1383-1385.
- Heusser, C. J. (1960). "Late-Pleistocene environments of North Pacific North America." American Geographical Society Special Publication 35.
- Ives, P. C., Levin, Betsy, Oman, C. L., and Rubin, Meyer (1967). U.S. Geological Survey radiocarbon dates IX. *Radiocarbon* 9, 505-529.
- Lowe, J. J., Lowe, S., Fowler, A. J., Hedges, R. E. M., and Austin, T. J. F. (1988). Comparison of accelerator and radiometric radiocarbon measurements obtained from Late Devensian Lateglacial lake sediments from Llyn Gwernan, North Wales, UK. *Boreas* 17, 355-369.
- Mann, D. H. (1983). "The Quaternary history of the Lituya glacial refugium, Alaska." Unpublished Ph.D. dissertation, University of Washington.
- Mann, D. H., (1986). Wisconsin and Holocene glaciation of southeast Alaska. In "Glaciation in Alaska, the Geologic Record" (T. D. Hamilton, K. M. Reed, and T. M. Thorson, Eds.), pp 237-265. Alaska Geological Society, Anchorage.
- Mann, D. H., and Ugolini, F. C. (1985). Holocene glacial history of the Lituya District, southeast Alaska. *Canadian Journal of Earth Sciences* 22, 913-928.
- McKenzie, G. D. (1970). Some properties and age of volcanic ash in Glacier Bay National Monument. *Arctic* 23, 46-49.
- Riehle, J. R. (1985). A reconnaissance of the major Holocene tephra deposits in the upper Cook Inlet region, Alaska. *Journal of Volcanology and Geothermal Research* 26, 37-74.
- Riehle, J. R., and Brew, D. A. (1984). Explosive latest Pleistocene (?) and Holocene activity of the Mount Edgecumbe volcanic field, Alaska. In "The United States Geological Survey in Alaska: Accomplishments during 1982" (K.M. Reed and Susan Bartsch-Winkler, Eds.), pp. 111-115. U.S. Geological Survey Circular 939.
- Riehle, J. R., Brew, D. A., and Lanphere, M. A. (1989). "Geologic map of the Mount Edgecumbe Volcanic Field, Kruzof Island, Southeastern Alaska." U.S. Geological Survey Miscellaneous Investigations Map I-1983.
- Rossman, D L. (1959). "Geology and Ore Deposits of Northwestern Chichagof Island, Alaska." U.S. Geological Survey Bulletin 1058-E, 139-216.
- Sarna-Wojcicki, A. M., Bowman, H. R., Meyer, C. E., Russell, P. C., Asaro, F., Michael, H., Rowe, J. J., Baedeker, P. A., and McCoy, G. (1980). "Chemical Analyses, Correlations, and Ages of Late Cenozoic Tephra Units of East-Central and Southern California." U.S. Geological Survey Open-File Report 80-231.
- Sarna-Wojcicki, A. M., Shipley, S., Waitt, R. B., Jr., Dzurisin, D., and Wood, S. H. (1981). Areal distribution, thickness, mass, volume, and grain-size of air-fall ash from the six major eruptions of 1980. In "The 1980 Eruptions of Mount St. Helens" P.W. Lipman and Mullineaux, D.R., Eds.), pp. 577-600. U.S. Geological Survey Professional Paper 1250.
- Smith, D. G. W., and Westgate, J. A. (1969). Electron probe technique for characterizing pyroclastic deposits. *Earth and Planetary Science Letters* 5, 313-319.
- Yehle, L. A. (1974). "Reconnaissance Engineering Geology of Sitka and Vicinity, Alaska, with Emphasis on Evaluation of Earthquake and Other Geologic Hazards." U.S. Geological Survey Open-File Report 74-53.